Supporting Information

Leveraging Gibbs Ensemble Molecular Dynamics and Hybrid Monte Carlo/Molecular Dynamics for Efficient Study of Phase Equilibria

Thomas E. Gartner, III,[1] Thomas H. Epps, III,*[,1,2] Arthi Jayaraman*[,1,2]

[1]Department of Chemical and Biomolecular Engineering, University of Delaware, 150 Academy Street, Newark DE, 19716

[2]Department of Materials Science and Engineering, University of Delaware, 201 DuPont Hall, Newark DE, 19716

*Corresponding authors thepps@udel.edu, arthij@udel.edu

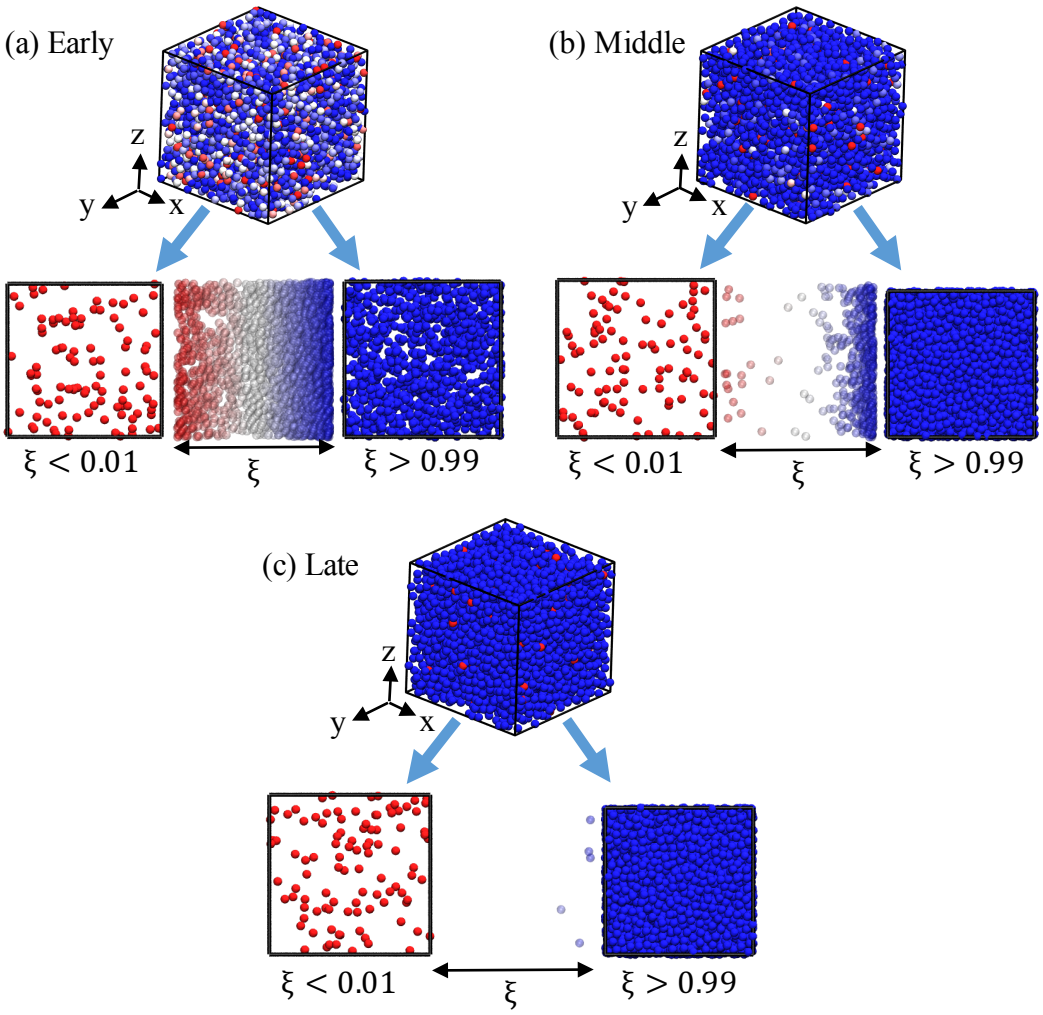

Figure S1. Snapshots from Gibbs ensemble molecular dynamics (GEMD) with a thermostat applied in the ξ space during early (a), middle (b), and late (c) stages of the simulation. ξ is a fourth positional degree of freedom and controls whether a bead is treated as existing in the liquid ($\xi > 0.99$) or vapor ($\xi < 0.01$) phase. Red represents vapor phase beads, blue represents liquid phase beads, and white represents transition state beads ($0.01 \leq \xi \leq 0.99$). The top snapshot in each subfigure illustrates all the components in the system (both liquid and gas phase) that share the same Cartesian space. In the lower snapshots for each subfigure, the system is separated along the ξ coordinate, with the vapor phase in the leftmost box, the liquid phase in

the rightmost box, and transition state arranged from left to right in the central box according to the value of the ξ coordinate of each bead.

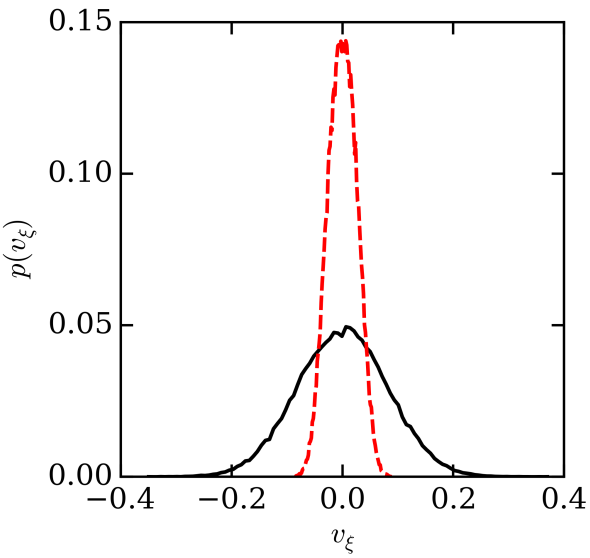

Figure S2. Probability distribution of velocities in the ξ space (v_ξ) for the 'without ξ thermostat' (black line) and 'with ξ thermostat' (red dashed line) versions of GEMD at a reduced temperature of T^* = 1.0. The 'without ξ thermostat' distribution corresponds to an average 'ξ temperature' of T_ξ = 1.0, and the 'with ξ thermostat' version corresponds to T_ξ = 0.1.

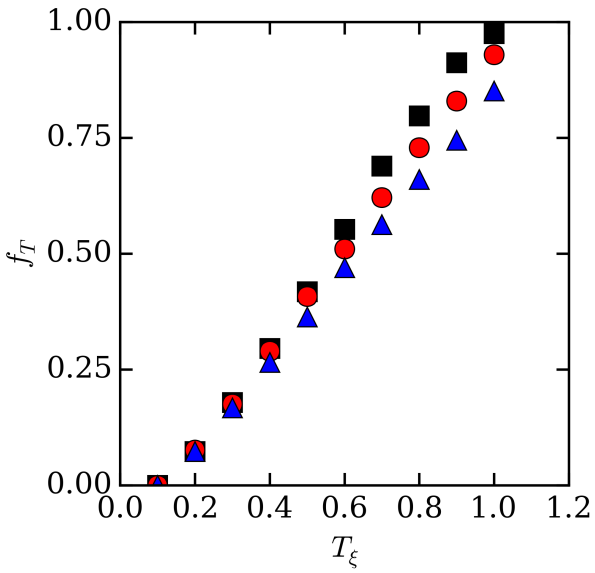

Figure S3. Fraction of total beads in the transition state (f_T), as a function of T_ξ for $T^* = 0.9$ (black squares), $T^* = 1.0$ (red circles), and $T^* = 1.1$ (blue triangles). The number of beads in the transition state decreases with increasing T^* for a given T_ξ. For the purposes of analysis, atoms are defined as in the transition state if their ξ coordinate lies in the range, $0.01 \leq \xi \leq 0.99$. When the T_ξ is low (i.e., less than $T_\xi = 0.1$), atoms are strongly partitioned into the liquid and vapor phases and do not have enough kinetic energy in the ξ space to enter the region $0.01 \leq \xi \leq 0.99$, resulting in a finite T_ξ but with $f_T = 0$.

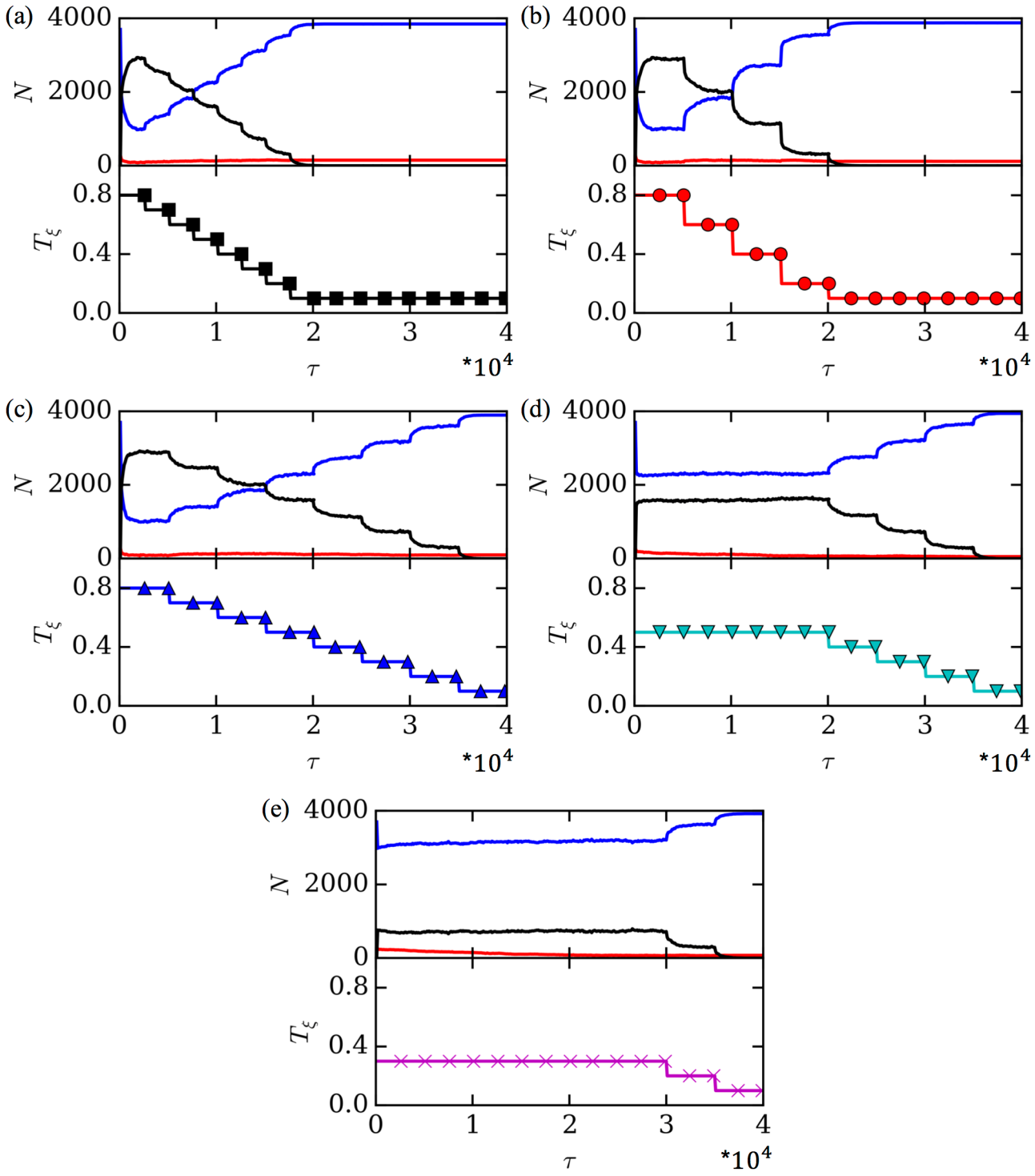

Figure S4. Near equilibrium - Number of beads (*N*) in the liquid phase (blue lines), vapor phase (red lines) and transition state (black lines) as a function of time (reduced time units $\tau = \sqrt{\frac{\epsilon}{m\sigma^2}}t$,

in which ε and σ are the Lennard-Jones parameters, m is the mass of a bead, and t is time) for various ξ annealing schedules (T_ξ versus τ), starting from an initial condition with 7.5% of beads in the vapor phase. The time evolution of N and the corresponding annealing schedule are plotted on the upper and lower plots, respectively, of each subfigure. Annealing schedules 1 (a), 2 (b), and 3 (c) have a maximum T_ξ of 0.8, and T_ξ decreases by 0.1 (a, c) or 0.2 (b) every 2.5×10^3 τ (a) or 5.0×10^3 τ (b, c). Annealing schedule 4 (d) has a maximum T_ξ of 0.5, and T_ξ decreases by 0.1 every 5.0×10^3 τ, starting at $\tau = 2.0 \times 10^4$. Annealing schedule 5 (e) has a maximum T_ξ of 0.3, and T_ξ decreases by 0.1 every 5.0×10^3 τ, starting at $\tau = 3.0 \times 10^4$. Because the initial condition is near the equilibrium condition, the system is not sensitive to the choice of annealing schedule, as all five annealing schedules achieved approximately the same final distribution of beads in the liquid phase, vapor phase, and transition state.

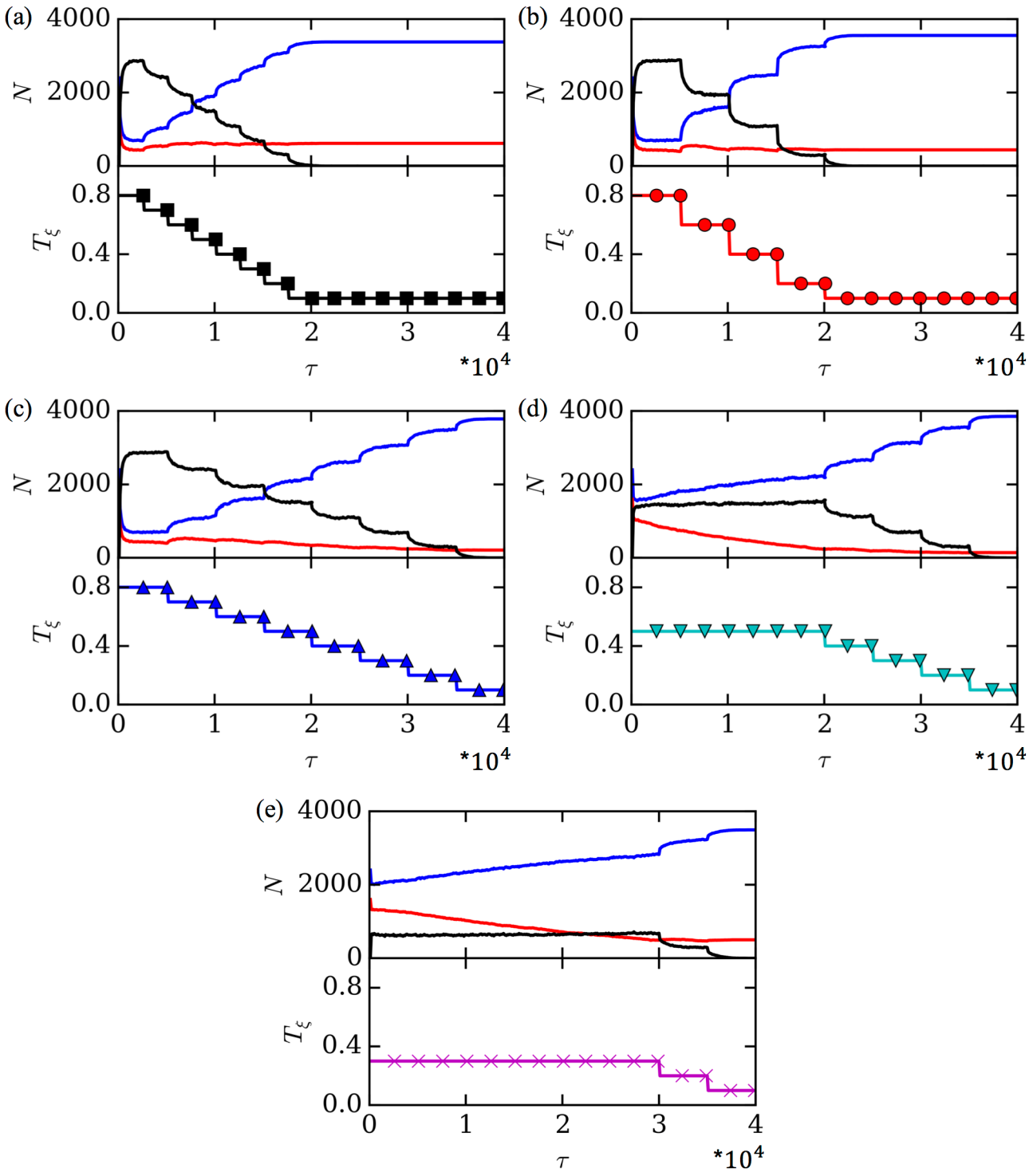

Figure S5. Far from equilibrium - Number of beads (*N*) in the liquid phase (blue lines), vapor phase (red lines) and transition state (black lines) as a function of time for various ξ annealing

schedules, starting from an initial condition with 40% of beads in the vapor phase. The time evolution of N and the corresponding annealing schedule are plotted on the upper and lower plots, respectively, of each subfigure. Annealing schedules 1 (a), 2 (b), and 3 (c) have a maximum T_ξ of 0.8, and T_ξ decreases by 0.1 (a, c) or 0.2 (b) every 2.5 x 10^3 τ (a) or 5.0 x 10^3 τ (b, c). Annealing schedule 4 (d) has a maximum T_ξ of 0.5, and T_ξ decreases by 0.1 every 5.0 x 10^3 τ, starting at τ = 2.0 x 10^4. Annealing schedule 5 (e) has a maximum T_ξ of 0.3, and T_ξ decreases by 0.1 every 5.0 x 10^3 τ, starting at τ = 3.0 x 10^4. Because the initial condition is far from the equilibrium condition, the system is sensitive to the choice of annealing schedule, as annealing schedules 1 (a) and 2 (b) resulted in different distributions of atoms between phases than those achieved by annealing schedules 3 (c), 4 (d), and 5 (e).

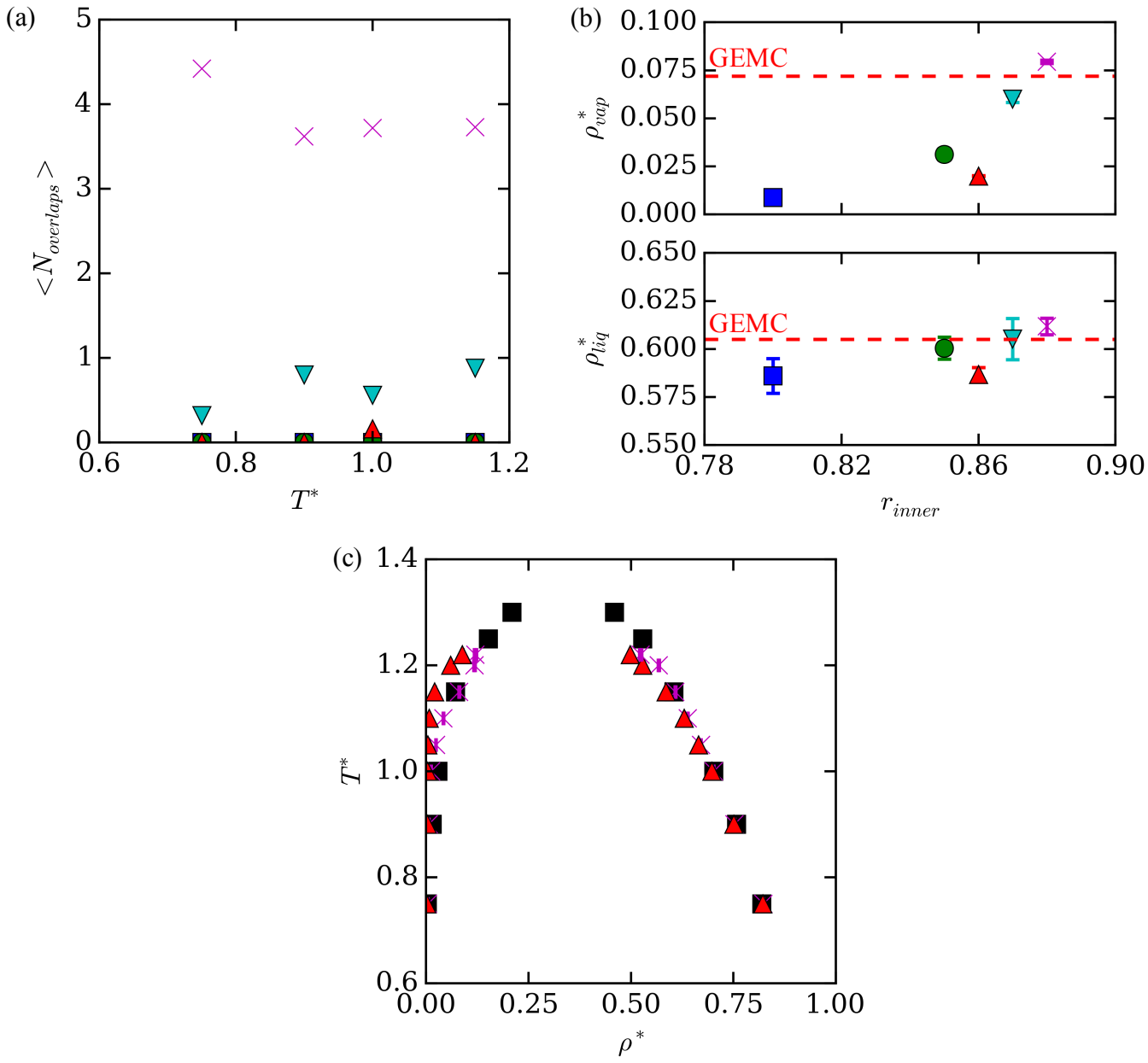

Figure S6. (a) Average number of atomic overlaps per timestep for the GEMD method with an inner cutoff to the intermolecular potential $r_{inner} = 0.80\ \sigma$ (blue squares), $r_{inner} = 0.85\ \sigma$ (green circles), $r_{inner} = 0.86\ \sigma$ (red triangles), $r_{inner} = 0.87\ \sigma$ (cyan triangles), $r_{inner} = 0.88\ \sigma$ (magenta crosses). (b) Coexistence densities for the Lennard-Jones fluid from the GEMD method at $T^* = 1.15$ for various values of r_{inner}. Gibbs ensemble Monte Carlo (GEMC) result from

Panagiotopoulos *et al.* at $T^* = 1.15$ is marked by the red dotted line.[1] (c) Phase diagram for the Lennard-Jones fluid from the GEMD method with $r_{inner} = 0.86\,\sigma$ (red triangles), $r_{inner} = 0.88\,\sigma$ (magenta crosses), and the GEMC method (black squares).[1] An inner cutoff of $r_{inner} = 0.88\,\sigma$ agrees more closely with the GEMC results, particularly at high temperatures. The critical point density (ρ_c^*) and temperature (T_c^*) were determined by fitting the law of rectilinear diameters[2] with critical exponent $\beta = 0.32$ to all data points $T^* \geq 0.9$, yielding $\rho_c^* = 0.268$ and $T_c^* = 1.28$ for $r_{inner} = 0.86\,\sigma$, $\rho_c^* = 0.319$ and $T_c^* = 1.27$ for $r_{inner} = 0.88\,\sigma$, and $\rho_c^* = 0.324$ and $T_c^* = 1.31$ for GEMC.

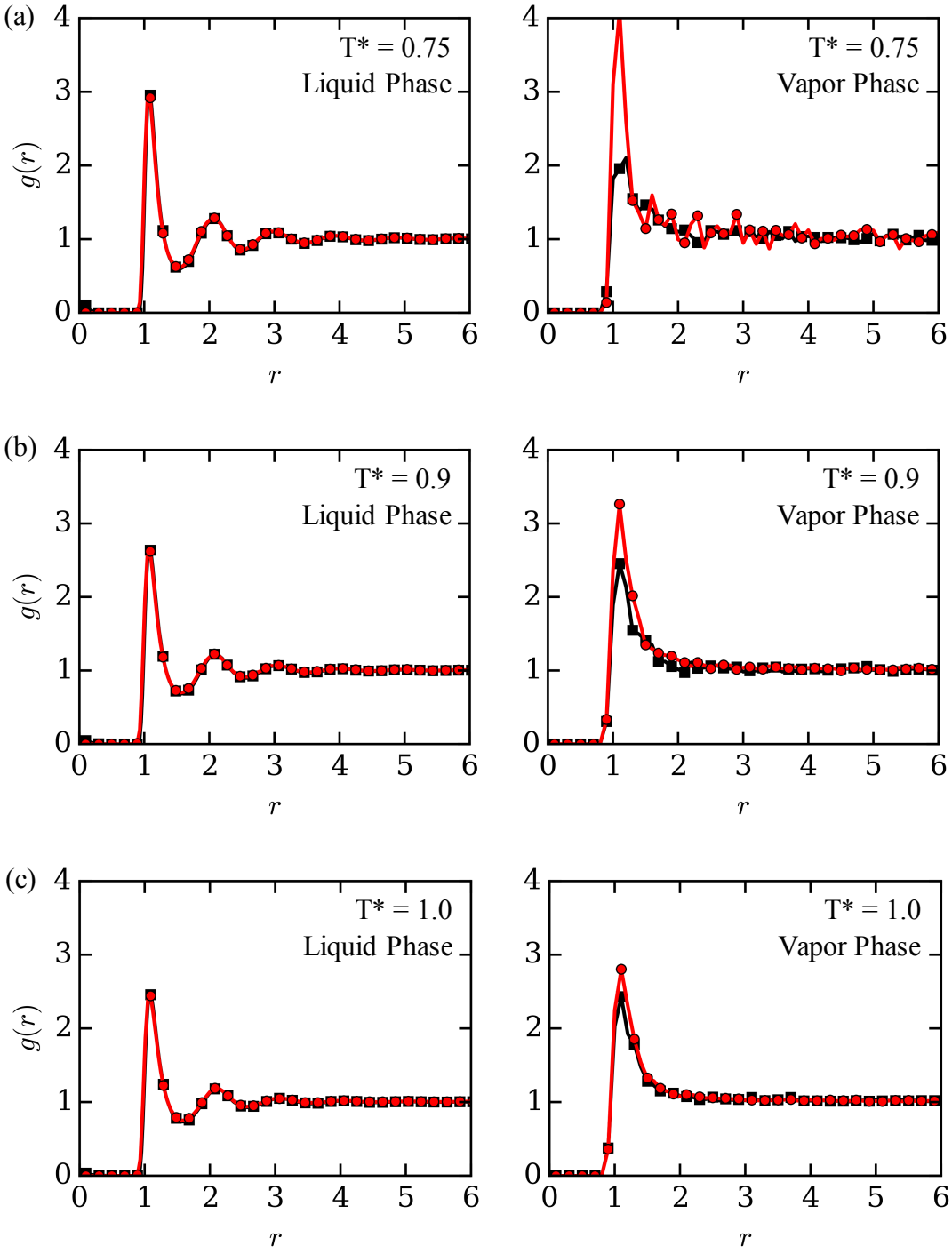
(a)
T* = 0.75
Liquid Phase
T* = 0.75
Vapor Phase
(b)
T* = 0.9
Liquid Phase
T* = 0.9
Vapor Phase
(c)
T* = 1.0
Liquid Phase
T* = 1.0
Vapor Phase
g(r)
r

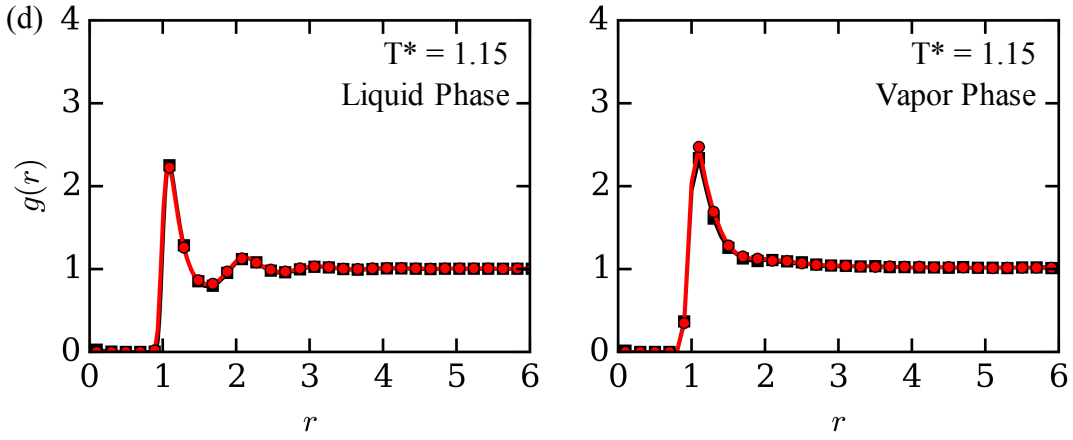

Figure S7. Liquid (left plots) and vapor (right plots) phase radial distribution functions [g(r)] at equilibrium for the GEMD (black lines and squares) and hybrid Monte Carlo/molecular dynamics (red lines and circles) methods at $T^* = 0.75$ (a), $T^* = 0.9$ (b), $T^* = 1.0$ (c), and $T^* = 1.15$ (d). The liquid phase g(r) agrees closely between both methods for all temperatures. The discrepancy in the height of the first peak of the vapor phase g(r) between the two methods is an artifact of the high degree of statistical uncertainty resulting from the small number of atoms in the vapor phase at low temperatures (a, b). At higher temperatures (c, d), the agreement in vapor phase g(r) between the two methods improves as the number of vapor phase beads increases, and the statistical uncertainty decreases.

Table S1. Vapor and Liquid Phase Densities for our Modified GEMD, our Hybrid MC/MD, GEMC,[a] and Hentschke *et al.* GEMD[b] methods.

T^*	ρ^*_{vap}				ρ^*_{liq}			
	GEMD	Hybrid	GEMC	Hentschke GEMD	GEMD	Hybrid	GEMC	Hentschke GEMD
1.3	--	0.230 (6)[c]	0.21 (1)	--	--	0.461 (7)	0.46 (3)	--
1.25	--	0.161 (5)	0.152 (3)	0.205	--	0.533 (7)	0.529 (9)	0.516
1.15	0.083 (1)	0.073 (3)	0.072 (9)	0.0692	0.608 (2)	0.606 (4)	0.605 (9)	0.602
1.0	0.0128 (3)	0.029 (2)	0.0283 (5)	0.0432	0.702 (1)	0.701 (4)	0.703 (3)	0.697
0.9	0.0072 (5)	0.014 (4)	0.0151 (3)	0.0233	0.0753 (1)	0.750 (3)	0.758 (9)	0.750
0.75	0.0049 (3)	0.0032 (7)	0.0031 (3)	--	0.823 (5)	0.821 (1)	0.819 (3)	--

[a] GEMC results from Panagiotopoulos *et al.*[1]
[b] GEMD results from Hentschke *et al.*[3]
[c] Numbers in parentheses are uncertainties in the last digit calculated through the standard deviation of 10 block averages

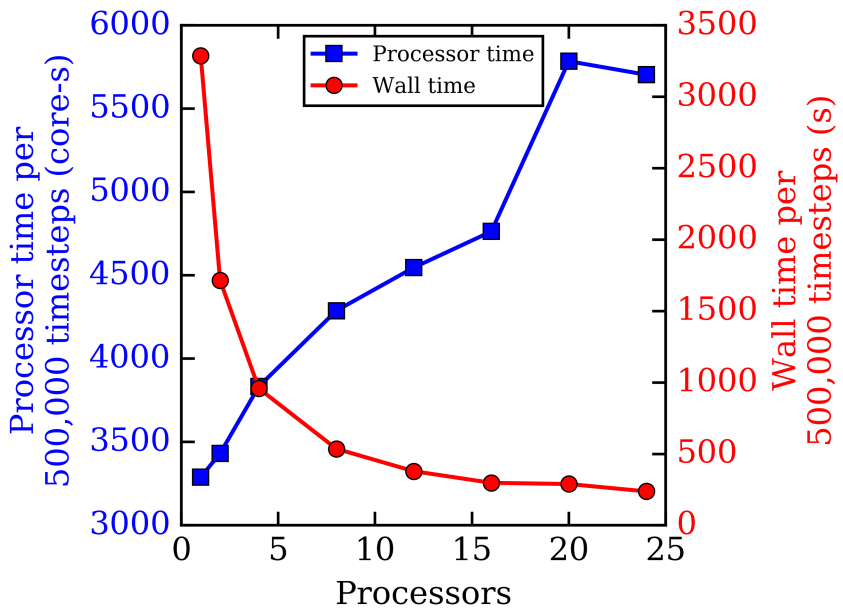

Figure S8. Performance scaling as a function of number of processors for the GEMD method at $T^* = 1.0$ with 4000 atoms. The right axis is the wall time needed to complete 500,000 GEMD timesteps (timestep size = 0.001 τ), and the left axis is processor time (wall time multiplied by number of processors) for 500,000 GEMD timesteps. These scaling simulations were performed on 2.5 GHz Intel Ivy Bridge CPUs on the University of Delaware Farber Supercomputing cluster, which has 100 compute nodes of 20 cores each.

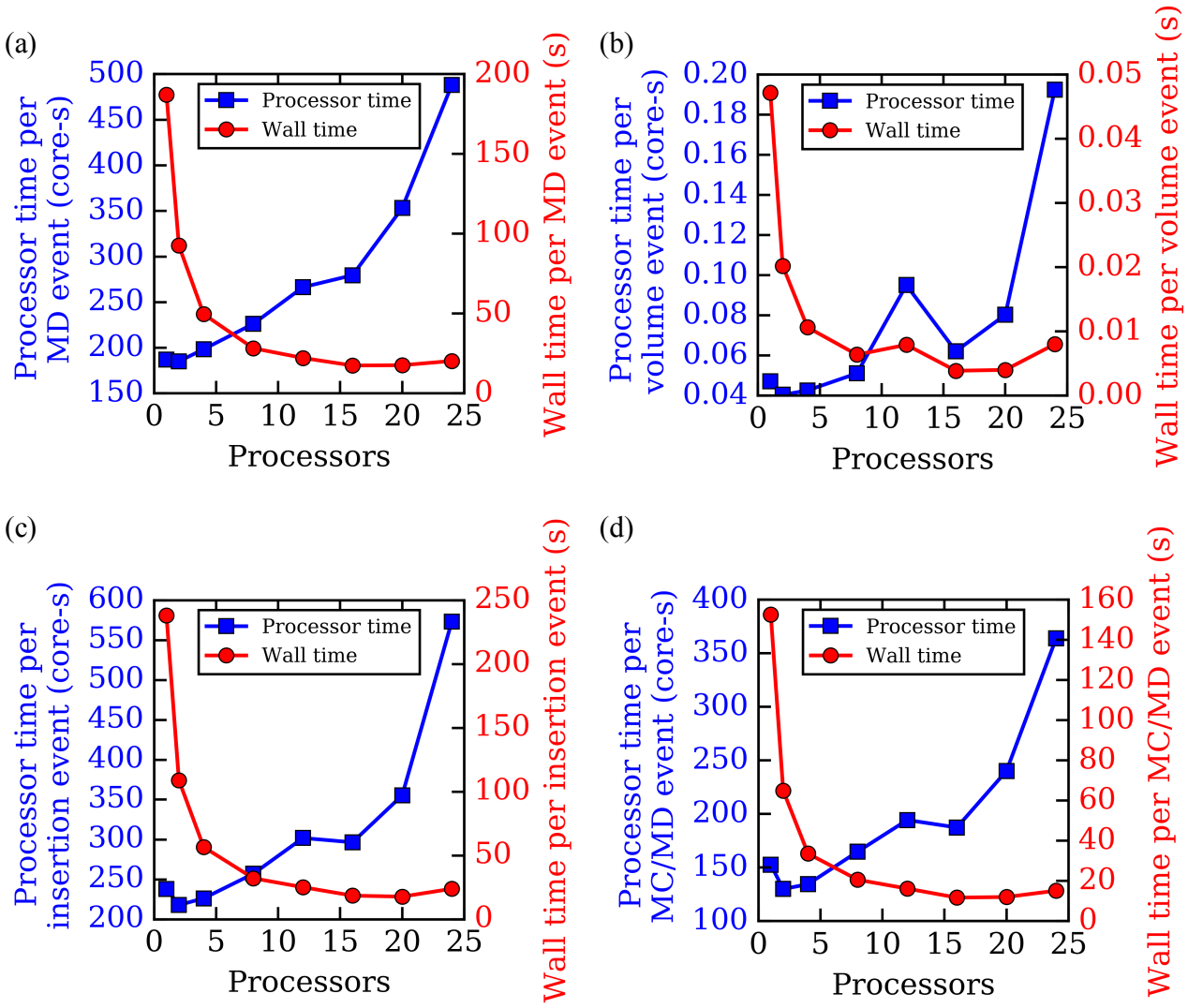

Figure S9. Performance scaling as a function of number of processors for the hybrid Monte Carlo/molecular dynamics (MC/MD) method at $T^* = 1.0$ with 4000 atoms, number of MD timesteps per event $N_{MD} = 50{,}000$ (timestep size = 0.001 τ), and number of trial particle exchanges per event $N_{exchange} = 4000$. The right axis of each plot is the average wall time needed to complete one MD event (a), one volume exchange event (b), one particle exchange event (c), or the average over all MC/MD events (d), and the left axis of each plot is processor time (wall time multiplied by number of processors). These scaling simulations were performed on 2.5

GHz Intel Ivy Bridge CPUs on the University of Delaware Farber Supercomputing cluster, which has 100 compute nodes of 20 cores each.

References

1. Panagiotopoulos, A. Z.; Quirke, N.; Stapleton, M.; Tildesley, D. J., *Mol. Phys.* **1988,** *63* (4), 527-545.
2. Frenkel, D.; Smit, B., *Understanding Molecular Simulation: From Algorithms to Applications*. 2nd ed.; Academic Press: San Diego, 2002.
3. Hentschke, R.; Bast, T.; Aydt, E.; Kotelyanskii, M., *J. Mol. Model.* **1996,** *2* (9), 319-326.